Some Applications of X and γ-Rays Dedicated Computerized Tomography Scanner in Agriculture

JOÃO DE MENDONÇA NAIME, PAULO ESTEVÃO CRUVINEL, ÁLVARO MACEDO DA SILVA, SILVIO CRESTANA AND CARLOS MANOEL PEDRO VAZ

Embrapa Agricultural Instrumentation

P.O.Box 741, 13560-970 – São Carlos, SP – Brazil

Abstract: - X and γ-rays computerized tomography (CT) is becoming a popular method of obtaining cross-sectional images of objects. Many commercial CT scanners using continuous spectrum from either an X-ray tube or γ-ray source are now available, mainly for medical use. Beyond its use in medicine, CT technique is now being widely used for nonmedical applications. However, the complexity and high cost and mainly its response in energy greatly limit nonmedical applications of CT scanner. Besides, medical CT scanners are constantly in use exclusively for patients. In 1987 the Center for Instrumentation of the Brazilian Enterprise for Agricultural Research Center (EMBRAPA) developed an X and γ-rays computerized minitomography scanner for multidisciplinary use. Since then, several multidisciplinary projects have been carried out mainly related to soil physics applications. Additionally, in 1994 and 1997 the Center developed a portable γ-ray computerized tomography scanner for field applications and an X-ray computerized microtomography scanner for high revolution imaging. In the present study, the importance of dedicated CT scanner use and data processing is demonstrated for evaluation of agricultural problems.

Key-Words: - Computerized Tomography, instrumentation, X-ray, gamma-ray, Soil Science

CSCC'99 Proceedings: - 4951-4957

1 Introduction

Nondestructive testing practitioners challenged by complex product testing may choose to use sophisticated methods and systems, e.g., computerized tomography, emission tomography or magnetic resonance imaging systems, developed for unrelated applications. CT permits imaging of objects in axial cross sections, a technique pioneered by Cormack [1] and Hounsfield [2]. In CT, axial images can be stored in the form of a stack of two-dimensional (2D) matrix of numbers [3]. When a narrow beam of monoenergetic photons with energy E and incident photon flux intensity (number of photons/unit time and area) N_0 passes through a nonhomogeneous absorber of thickness x [cm], then the emerging photon intensity will be given by:

$$N = N_0 \exp \oint_s \left(-m\left(r, Z, E\right)x\right)ds \tag{1}$$

where μ [cm^{-1}] is the linear attenuation coefficient for material of physical density ρ (g/cm^3) and atomic number Z. The total linear attenuation coefficient is given by:

$$m_{tot} = m_{ph} + m_c + m_r + m_p \tag{2}$$

where μ_{ph}, μ_c, μ_r, and μ_p, respectively designate photoelectric effect, Compton scattering, Rayleigh scattering and pair production. Although linear attenuation coefficients are convenient for engineering applications and shielding calculations, they are proportional to the density of the absorber, which depends on the physical state of the material. Since molecular binding energies are smaller than energies involved in X-ray radiography and tomography, a reasonable approximation assumes that the linear attenuation coefficient is directly proportional to physical density. If the absorber is a chemical compound or mixture, its mass attenuation coefficient μ/ρ can be approximately evaluated from the coefficients for the constituent elements according to the weighted sum:

$$\frac{m}{r} = \sum w_i \left(\frac{m_i}{r_i}\right) \tag{3}$$

where w_i is the proportion by weight of the i-th constituent the material. The mass attenuation coefficient of a compound or a mixture can be, therefore, calculated from the mass attenuation coefficient of the components.

However, it should be emphasized that CT systems are optimized by design for specific applications and therefore both hardware and software should be analyzed carefully before being used for a new application. For example, medical CT systems conveniently available in most hospitals offer advantages over traditional nondestructive testing methods, in evaluating both high and low density materials. Satisfactory use of medical CT demands thorough understanding of both measurements systems and signal-processing algorithms. Otherwise, the tomographies may be either distorted or low-contrast, resulting in misinterpretation of the examined materials.

Computerized tomography, as a new method for investigation in soil science physics, was introduced by Petrovic et al. [4] in 1982, Hainsworth and Aylmore in 1983 [5], and by Crestana et al. in 1984 [6]. Petrovic demonstrated the possibility of using X-ray transmission computed tomography to measure soil bulk density. Crestana demonstrated that CT can also be applied not only for measuring water content of soil but also to follow dynamically water motion in soil in three dimensions. Also, using a third-generation CT scanner, several techniques can be applied, such as differential tomography and real time and spatial distribution scanning modes. Linear dependence was demonstrated for the Hounsfield units (HU) used in CT and water content. The application of CT methodology in soil science has proven to be of great advantage when compared to other classical methods such as gravimetry or γ-ray direct transmission [7]. CT can measure local heterogeneity within soil at pixel resolution, soil bulk density, and water content pixel by pixel, or even noninvasively obtain two or three-dimensional images of soil samples independent of the geometry of each sample. Two and three-dimensional measurement of physical parameters of soil such as bulk density and water content is an important task in modeling and analyzing soil science problems. In agriculture, a need exists for nondestructive experimental techniques with millimeter or submillimeter resolution capable of investigating intricacies present in the variety of processes occurring in soil. Some examples of coupled and time-dependent soil processes are compaction; root penetrations; crusting; seedling cracking and swelling; wetting/drying or thawing/freezing cycles; miscible and unmiscible displacement of nutrients in the presence of roots; and preferential flow of pollutants in fractured porous media. CT is becoming a powerful tool for studying such soil phenomena shows the linear attenuation coefficient of soil, water and SiO_2 as a function of incident energy (Fig. 1), where the mean error ranges from 2% to 4% [8]. It is important to observe that the difference in linear attenuation coefficient for different materials is energy dependent, which leads to the definition of CT image contrast. Despite the high cost of medical CT scanners and because they are dedicated to patients use, X-ray energy used in such systems is suitable for medical diagnostics.

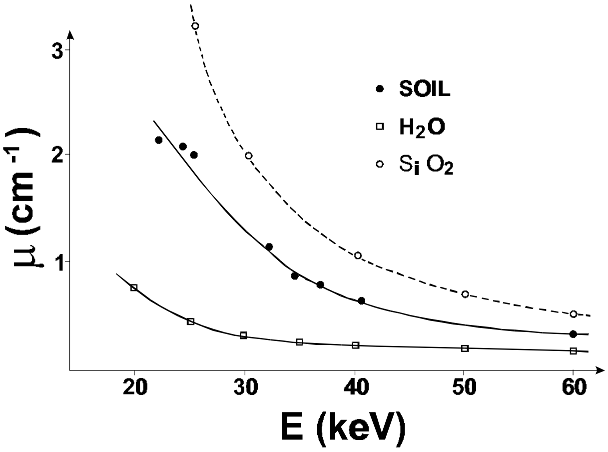

Fig. 1 – The linear attenuation coefficient of soil, water and SiO_2 as a function of incident energy (after Crestana el al., 1986).

In 1987 Cruvinel [9] [10] developed an X and γ-ray computerized minitomograph scanner for multidisciplinary purposes with the possibility of using several different beam energies and radioactive sources as well as X-ray fluorescent targets. In 1989 Vaz et al. demonstrated the usefulness dedicated systems for studying tillage-induced soil compaction [11].

In 1994 Naime [12] [13] developed a portable γ-ray computerized tomography scanner, which can be used directly in the field. Moreover, in 1997, Macedo [14] [15] developed an X-ray computerized tomography scanner for high-resolution imaging.

This report describes the usefulness of dedicated CT scanners for analyzing some agriculture-related problems.

2 Some Applications of X and γ-Ray Tomography in Agriculture and Discussion

2.1 Application in Soil Science Analysis

The dedicated mini-CT scanner from EMBRAPA Agricultural Instrumentation has been used to measure soil bulk density. The range of soil bulk densities studied was from 0.96 to 1.55 g/cm^3 in soil samples collected from an agricultural field in Brazil. The collimators used in the experiment had a window size of 1mm near the radioactive source and 1 mm in front of the detector. The distance between the source and detector was 15 centimeters. Energy of 59.5 keV was used and the counter was adjusted to allow data collection for tomographic projections with 10 seconds intervals. Each 80x80 pixels image followed upon reconstruction by the Fourier filtered inversion methodology in approximately 20 milliseconds.

In addition, a set of soil bulk density values was obtained for air-dried soil samples of non-swelling latosol. Fig. 2 shows the image produced by the dedicated mini-CT scanner for a soil.

The attenuation at the cross section of soil employed in this experiment was 0.433 cm^2/g and the mass attenuation coefficient was constant with density, indicating prevalence of the Compton effect at 59.5 keV. Soil bulk density analysis with spatial resolution on a millimeter scale, besides costing less is, of course, more precise than classical agricultural methodologies, where the meter scale is still common.

2.2 Application to wood density analysis

As a consequence of ecological problems generated by wood extraction from native forests, reduction of pine and latifoliate forests and the rising costs of transport from the amazon rainforest, wood obtained from reforestation plays an important role in supplying the timber industries of southern and southeastern Brazil.

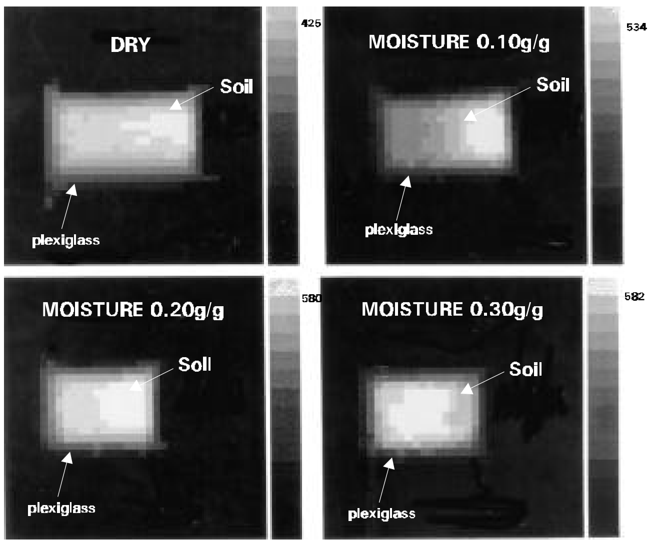

Fig. 2 – Tomographic images obtained from soil samples at 59.5keV.

The search for alternative trees, e.g. *Eucalyptus* and *Pinus*, to substitute traditional species used in the furniture industry and civil construction is an intense demand. Although the available experimentation permits to identify various promising species, the lack of technical information has limited the use of these woods.

This situation is due to the fact that techniques applied until now are destructive, time consuming and mostly imprecise and, consequently further studies are necessary for genetic improvement programs and wood quality analysis by reforestation enterprises.

Among the parameters used to evaluate wood quality, density (dry wood mass per total volume) stands out as a consequence of its strong technological and economic significance. This parameter indicates shrinkage and swell, mechanical resistance, production and quality of pulp, production and quality of coal, as well operational cost timber transport and the storage.

Traditional methods of determining wood density are gravimetric (measurement of sample mass and volume) and attenuation of a γ or X-ray beam. However, while these methods give the average density values of the sample as a whole, they do not allow analysis of internal variation, which is fundamental in the proposed study.

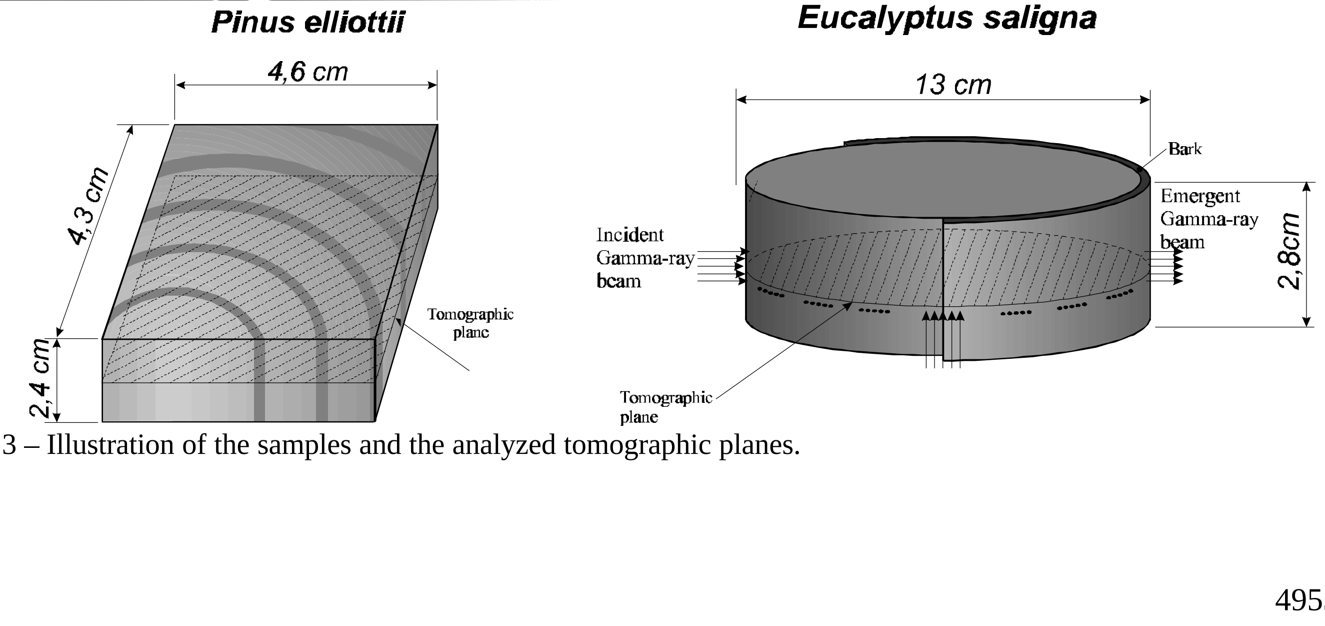

Fig. 3 – Illustration of the samples and the analyzed tomographic planes.

In this work, some preliminary results are presented to show the potentiality of the tomographic technique applied to wood density determination. Two samples (Fig. 3) from Paraná state – Brazil were analyzed: *Eucalypitus saligna* and *Pinus Elliottii* var. *elliottii*. Using a computerized tomograph developed in EMBRAPA [10]. Figs. 4 and 5 show the obtained tomographic images beside each respective density profile. Concerning the 59.5 keV energy from the γ-ray source ^{241}Am , the mass attenuation coefficient (μ_m - $cm^2.g^{-1}$) depends on sample composition. For the wood samples mentioned above, the μ_m obtained are 0.1886 $cm^2.g^{-1}$ and 0.1860 $cm^2.g^{-1}$ respectively for *Eucalyptus* and *Pinus*. The density thus is calculated: D = UT / (1000 μ_m), UT is the tomographic unit, a numerical value assigned to gray levels in the tomographic image. In the tomographic image of *Eucalyptus* (Fig. 4), one observes higher (A) and lower (B) density regions. Besides, it is visible a fissure, part of the bark and some regions of density variation delimiting growth rings. The density profile shows variations from 0.49 $cm^2.g^{-1}$ to 0.88 $cm^2.g^{-1}$. The average value is 0.7092 $g.cm^{-3}$ whereas that obtained from the gravimetric method is 0.7380 $g.cm^{-3}$.

The *Pinus* image (Fig. 5) clearly shows the growth rings with densities greater than the rest of the sample. Density values of 0.612 in the laterwood (autumn layers) and 0.30 $g.cm^{-3}$ in the earlywood (spring layers) were obtained. The average value in the profile is 0.3846$g.cm^{-3}$, very close to the 0.3890 $g.cm^{-3}$, calculated through the gravimetric method.

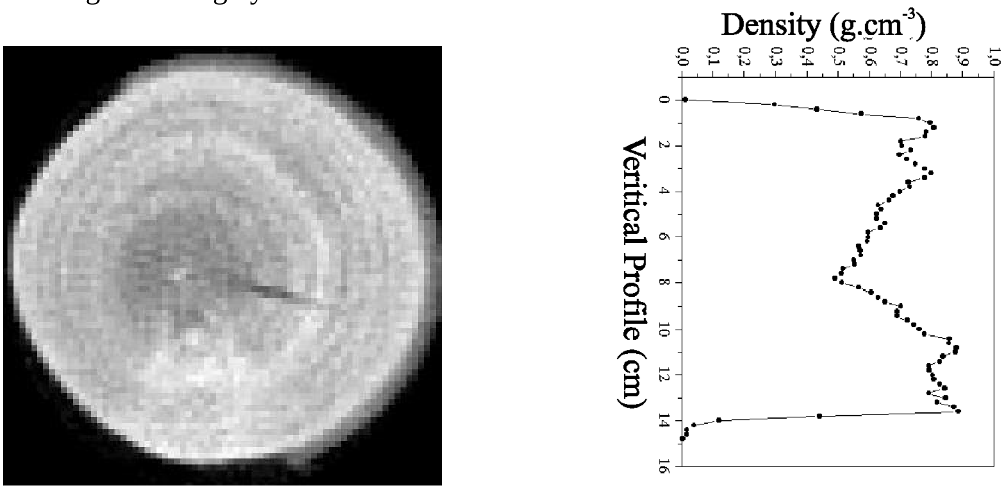

Fig. 4 – Tomographic image from the sample of E. saligna and its vertical profile of densities.

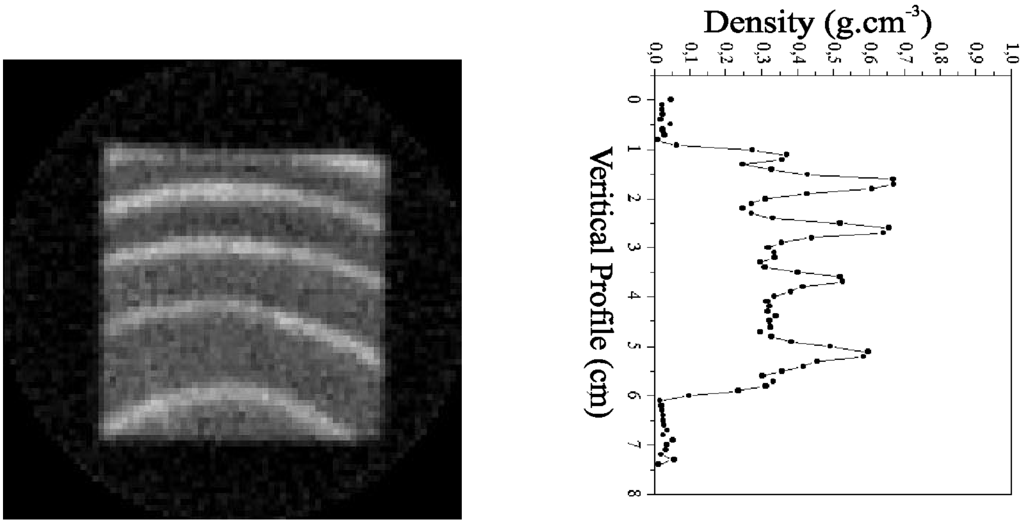

Figure 5 – Tomographic image from the sample of P. elliottii and its vertical profile of densities.

The results show that the data obtained from the tomographic images can easily be converted to densities and visually, geometrically and quantitatively analyzed. Moreover, can be determined whenever required statistical parameters like average, standard deviation, and histogram in any region of interest.

2.3 Soil Surface Sealing Study with Microtomography

Soil surface sealing a process caused by the impact on soil of raindrops or irrigation water, amounts to micro-bombardment. The drop after hitting the soil forms a micro-crater with some of the segregated fine soil particles relocating to clog pores, and the remainder washing deeper into the soil with infiltrating water. This process may drastically reduce water infiltration and, as a consequence, cause runoff and, therefore, erosion. There is not yet a consensus about the sealing process, making necessary further studies on the formation process and its influences on water infiltration and plant germination [16] [17] [18] [19] [20].

Macedo et al. [15] present a microtomography (Fig. 6) of a soil sample with soil sealing. The sample is dark red podzol, 32% clay, 8% silt and 54% sand. The samples of this parcel were sprinkler irrigated during one hour periods; and dried in the shade during 24 hours, between two consecutive irrigations. In this result, the formation of three layers is visible, the upper layer being more homogeneous and more compact than the others. The lowest layer presents porosity approximately twice that of the other two. Macroporosity, visually estimated in the middle layer, ranges from twice or three times greater than the others.

Two other results are presented in Figs. 7 and 8, in two microtomographies of a sample from the same plot as previous sample. In the first one, a sub-sample was extracted close to the original sample surface. In the second one, the sub-samples were taken from the center of sample.

In the evaluation of Fig. 7, the average tomographic units were computed inside rectangles 45 pixels wide and 3 pixels high. Table 1 shows the results from this evaluation. Higher densities are observable in the sample surface, since for applied energy, 59.5 keV, one can consider linear density variation with the tomographic units, for the soil.

Fig. 8 shows higher macroporosity compared to that shown in the surface tomography, however with higher density, even if the tomographic units are calculated disregarding the denser particles and including the macropores. While the average tomographic unit in Fig. 7 is 0.392, in Fig. 8 this value, calculated as described above, is 0.570.

These are the first results, further investigation is necessary to provide conclusive evaluation. Macedo et al. [15] presented a surface-only tomographic image at –3.2 mm depth. In this work, the first image was taken from a layer at –2.5 mm depth and the next layers from between –4.0 mm to -12.0 mm depth.

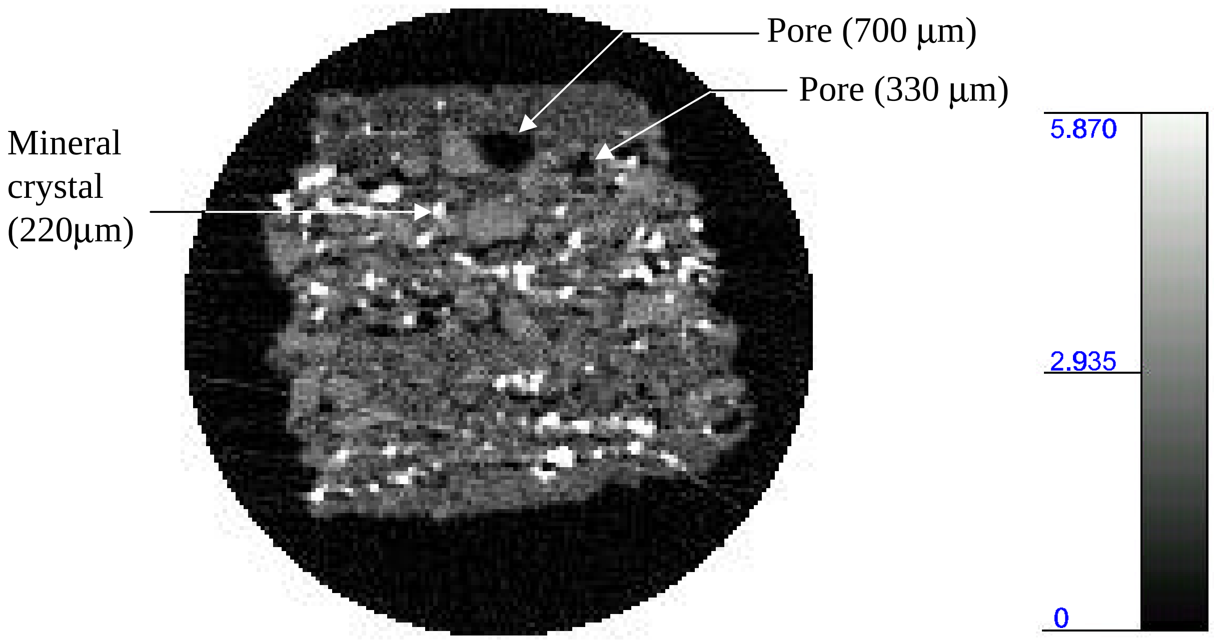

Figure 6 – Micrometric tomography of a soil with surface sealing. The macropores and mineral crystal can be observed.

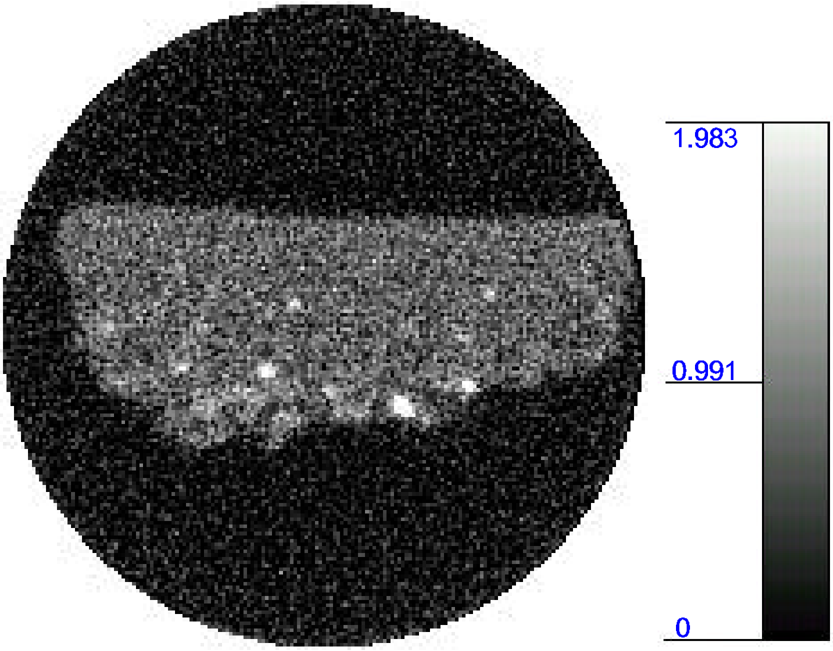

Fig. 7 – Microtomography of the top a soil sample with surface sealing.

Another evaluation planned in this work concerns the soil compaction phenomenon in the São Francisco river valley, in Petrolina/Pe Brazil. In the semi-arid of the northeast region of Brazil, the presence of dense and/or compacted layers is noticeable in podzol soils. Soils with this characteristic, submitted to irrigation, show very low infiltration rates and, consequently, momentary soaking, creating difficulties in soil and water management. One hypothesis for the presence of these layers is pedogenic, another suggests intense soil use.

Table Evaluation of tomographic units from a microtomography of a soil sample with soil sealing, presented in Fig. 7

Rectangle Center			**Rectangle Center**			**Rectangle Center**		
Column	**Row**	**T.U.**	**Column**	**Row**	**T.U.**	**Column**	**Row**	**T.U.**
44	61	0,417	107	63	0,394	152	63	0,412
44	64	0,384	107	66	0,398	152	66	0,399
44	67	0,407	107	69	0,379	152	69	0,405
44	70	0,389	107	72	0,378	152	72	0,371
44	73	0,399	107	75	0,370	152	75	0,400
44	76	0,379	107	78	0,345	152	78	0,391
44	79	0,387	107	81	0,385	152	81	0,409
44	82	0,380	107	84	0,383	152	84	0,368
46	85	0,402	107	87	0,389	152	87	0,379
48	91	0,417	107	90	0,374	152	90	0,368
48	94	0,380	107	93	0,390	152	93	0,352
49	97	0,371	107	96	0,357	152	96	0,358
50	100	0,388	107	99	0,348	152	99	0,338

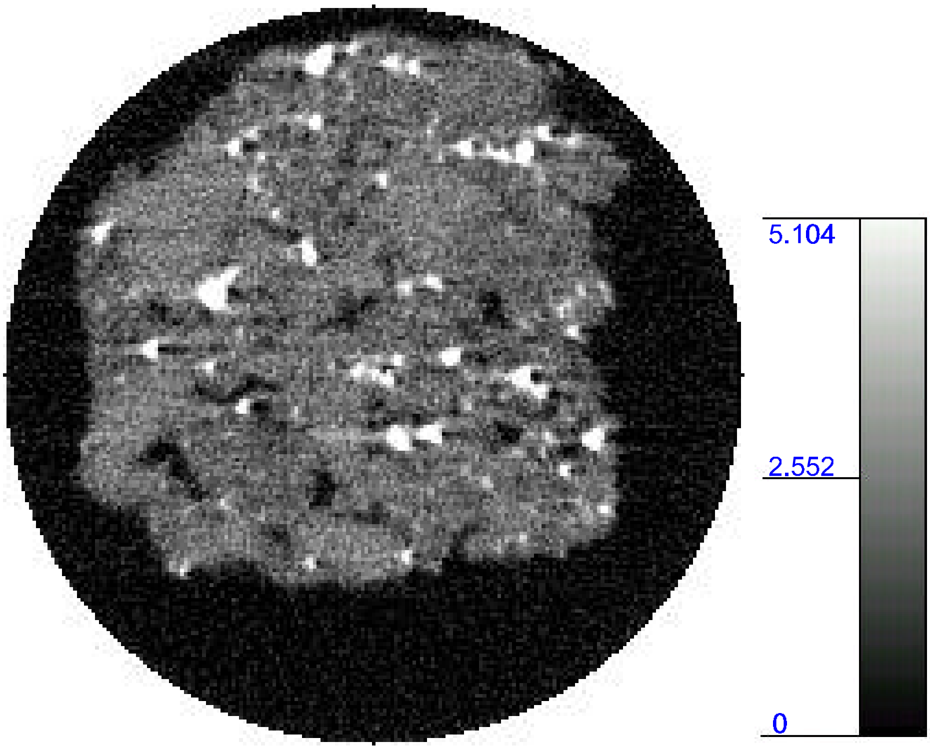

Fig. 8– Microtomography from a central part of a soil sample with soil sealing.

3. Conclusion

This study has demonstrated the viability and usefulness of the use of dedicated computerized tomography scanners in dealing with agricultural problems. Some examples of their use in soil science and wood density and surface sealing analysis were presented.

References:

[1] Cormack A. M., *Reconstruction of Densities From Their Projections with Applications In Radiological Physics*, Physics in Medicine and Biology, v. 18, Nº. 2, p. 195-207, 1973.

[2] Housfield G.N., *Computerized Transverse Axial Scanning (Tomography): Part 1. Description of System*, British Journal of Radiology. vv.46, p. 1016-1022, 1973.

[3] Cho, Z.H. & Chan, J.K., *A Comparative Study of 3-D Image Reconstruction Algorithms with Reference to Number of Projections and Noise Filtering* , IEEE Transactions. On Nuclear Science, v. NS-21, Nº. 1, p. 344-364, 1975.

[4] Petrovic A.M., Siebert J.E., and Rieke P.E., *Soil Bulk Density Analysis in Three Dimensions by Computed Tomographic Scanning*, Soil Water Content, Aust. Journal Soil Res., v. 21, p.445-450, 1982.

[5] Hainswortth J.M. and Aylmore L.A.G., *The Use of Computer-Assisted Tomography to Determine Spatial Distribution of Soil Water Content*, Aust. Journal Soil Res., v. 21, p.435-443, 1983.

[6] Crestana S., Mascarenhas S., and Pozzi-Mucelli R.S., *Static and Dynamic Three-Dimensional Studies of Water in Soil Using Computed Tomographic Scanning*, Soil Science, v. 140, Nº. 5, p. 326-332, 1985.

[7] Scwab G.º and Frevert R.K., *Elementary Soil and Water Engineering*, New York, Willey Publishing, 1985.

[8] Crestana S., Cesareo R., and Mascarenhas S., *Using a Computed Tomography Miniscanner in Soil Science*, Soil Science., V. 142, Nº. 1, p. 56-61, 1986.

[9] Cruvinel P.E., *X and Gamma Ray Computerized Mini-Scanner for Multidisciplinary Use*, Doctoral Thesis, University of Campinas, UNICAMP, SP, Brazil, pp. 329, 1987.

[10] Cruvinel P.E., Cesareo R., Crestana S., and Mascarenhas S., *X and Gamma Rays Computerized Minitomograph Scanner for Soil Science*, IEEE Trans. On Instrum. And Meas., v. 39, Nº. 5, p. 745-750, 1990.

[11] Vaz C.M.P., Crestana S., Mascarenhas S., Cruvinel P.E., Reichardt K., Stolf R., *Using a Computed Tomography Miniscanner for Studying Tillage Induced Soil Compaction*, Soil Technology, Cremlinger, v. 2, p. 313-321, 1989.

[12] Naime, J.M. *Project and construction of a portable tomography scanner for in situ soil science studies.* Master Thesis, University of São Paulo, USP-EESC, SP, Brazil, pp. 87, 1994.

[13] Naime, J.M.; Cruvinel, P.E.; Crestana, S.; Conciani, W.; Soares, M.M. *Portable CAT scanner applied to collapsible soil studies*. In: GAZZINELLI, R.; MOREIRA, R.L.; RODRIGUES, W.N., ed. *Physics and industrial development:* bridging the gap - proceedings of the 2nd International Conference, Belo Horizonte-MG, July 1997. Singapore: World Scientific, p.327-331, 1997.

[14] Macedo, A. *Construction and use of tomography scanner with micrometic resolution for soil science and environmental applications.* Doctoral Thesis. University of São Paulo, USP-EESC, SP, Brazil, pp. 129, 1997.

[15] Macedo, A.; Crestana, S.; Vaz, C:M:P: *X-ray microtomography to investigate thin layers of soil clod.* Soil Tillage, Amsterdam, v.49, n.3, p.249-253, 1998.

[16] Moore, D.C.; Singer, M.J. *Crust formation effects on soil erosion processes.* Soil Science Society of America Journal, 54:1117-1123, 1990.

[17] Rawls, W.J.; Brakensiek, D.L.; Simanton, J.R.; Kohl, K.D. *Development of a crust factor for a Green-Ampt model.* Transactions of the ASAE, 33:1224-1228, 1990.

[18] Fattah, H.A.; Upadhyaya, S.K., Effect of soil crust and soil compaction on infiltration in a Yolo loam soil. Transactions of the ASAE, 39: 79-84, 1996.

[19] Morin, J.; Van Winkel, J., *Effect of raindrop impact and sheet erosion on infiltration rate and crust formation*. Soil Science Society of America Journal, 60:1223-1127, 1996.

[20] Slattery, M. C.; Bryan, R. B., *Surface seal development under simulated rainfall on an actively eroding surface*. Catena Supplement 22, Catena Verlag, Cremlingen-Destedt, 22:17-34, 1994.